Advances in Geo-Energy Research

Vol. 11, No. 1, p. 54-73, 2024

Original article

Empirical correlations for density, viscosity, and thermal conductivity of pure gaseous hydrogen

Ehsan Heidaryan, Saman A. Aryana*

Department of Chemical & Biomedical Engineering, University of Wyoming, Laramie, WY 82071, USA

Keywords:
Pure hydrogen
thermodynamic properties
transport properties

Cited as:
Heidaryan, E., Aryana, S. A. Empirical correlations for density, viscosity, and thermal conductivity of pure gaseous hydrogen. Advances in Geo-Energy Research, 2024, 11(1): 54-73.
https://doi.org/10.46690/ager.2024.01.06

Abstract:
This study addresses the critical need for reliable tools to calculate the thermophysical properties of pure gaseous hydrogen across a wide range of temperatures and pressures. This work proposes accurate and user-friendly functions of temperature and pressure based on a meticulous analysis of an extensive dataset sourced from the open literature. These functions are designed to predict volumetric, transport, and derived properties. The dataset comprises 3,396 data points for density, 940 data points for viscosity, and 2,287 data points for thermal conductivity, covering an extensive temperature and pressure spectrum. For density, the data covers a temperature range from 97 to 873 K and pressures ranging from atmospheric to 1.983 GPa. Viscosity data span temperatures from 100 to 1,100 K and pressures from atmospheric to 217 MPa, while thermal conductivity data extend from 98 to 873 K, with pressures ranging from atmospheric to 99 MPa. The data have been meticulously curated to ensure reliability and representativeness. The proposed correlations exhibit exceptional accuracy, as evidenced by the Absolute Average Deviation results: 0.66% for density, 1.21% for viscosity, and 1.65% for thermal conductivity. To ensure the reliability, the correlations were validated against data from REFPROP 10. In addition to the absolute average deviations, maximum absolute deviations, Coefficients of Determination, and the Percentage of Accuracy-Precision are also included. The proposed correlations have been formulated and validated for a range of key parameters, including isothermal compressibility, volume expansion, fugacity coefficient, enthalpy, entropy, Helmholtz energy, Gibbs energy, adiabatic bulk modulus, speed of sound, as well as kinematic viscosity and thermal diffusivity.

1. Introduction

In addressing global warming, achieving net-zero emissions represents a pivotal milestone. This objective necessitates a comprehensive strategy that includes reducing dependence on fossil fuels, mitigating greenhouse gas emissions, and integrating various low-carbon energy systems. Among the potential solutions, hydrogen (H_2) stands out because its combustion does not produce carbon dioxide (CO_2), emitting only water as a byproduct (Goria et al., 2024). Fossil fuels remain the primary source for the global production of hydrogen was primarily derived from fossil fuels (IRENA, 2023). The CO_2 footprint of these conventional methods contrasts starkly with the potential of green H_2, produced through water electrolysis powered by renewable energy. Although green H_2 production is still in its infancy, its crucial role in achieving net-zero emissions should not be understated (Iberdrola, 2023; Xue et al., 2023).

Hydrogen energy conversion and storage offers benefits such as regulating the energy grid's intermittent renewable outputs and reducing CO_2 emissions (Chu et al., 2023). Unique properties of H_2, such as its high energy content of 33.3 kWh/kg, nearly three times that of gasoline (Katalenich and Jacobson, 2022), are vital for its broader acceptance as a sustainable energy source.

H_2 is under serious consideration as a potential dense energy carrier in various parts of the globe. The United Nations Industrial Development Organization emphasizes its utility in large-scale renewable energy storage, serving as

Yandy Scientific Press

*Corresponding author.
E-mail address: eheidary@uwyo.edu (E. Heidaryan); saryana@uwyo.edu (S. A. Aryana).

Received November 15, 2023; revised December 3, 2023; accepted December 24, 2023; available online December 28, 2023.

Table 1. Critical properties, acentric factor, and molar mass of H_2 and CH_4 (Elliott et al., 2023).

Compound	T_c (K)	p_c (MPa)	ρ_c (mole/L)	ω (-)	M (g/mole)
H_2	33.145	1.2964	15.508	-0.219	2.0159
CH_4	190.56	4.5992	10.139	0.01142	16.043
CO_2	304.13	7.3773	10.625	0.22394	44.01

a buffer to store excess energy and release it during peak demand (UNIDO, 2018). The significant carbon-reducing potential of H_2, particularly as a clean alternative to fossil fuels, is highlighted in the IPCC 1.5 °C Report (Huppmann and Smith, 2018). In the United States, projections suggest that H_2 could meet up to 14% of the nation's total energy demand by 2050 (IPCC, 2018), significantly reducing fossil fuel dependency.

The importance of H_2 extends beyond its energy applications. For instance, in the context of the Haber-Bosch process, approximately 3% of the world's natural gas production is used to produce hydrogen, which yields around 500 million tons of ammonia annually (Negro et al., 2023). Its roles in food industry refinement (Han et al., 2023), metallurgy (Qiu et al., 2023), and electronics (Nguyen et al., 2023) underscore its widespread significance. These multifaceted applications highlight the need for a comprehensive understanding of H_2 properties, especially as the world approaches a transformative juncture in the technological and energy sectors.

Considering H_2 is mainly produced on an industrial scale by steam methane reforming, Chen et al. (2023) concluded that understanding calculated properties, such as Gibbs, is vital to understanding and controlling reforming reactions. Accurate simulations of hydrogen's fate in cyclic subsurface storage operations hinge on reliable estimates of its thermophysical properties. These simulations are critical to assessing and optimizing underground hydrogen storage strategies, particularly in minimizing leakage risks and enhancing recovery efficiency (Zhang et al., 2023). Due to its relatively low viscosity and density, hydrogen exhibits high mobility, leading to potential unstable flow behavior and suboptimal storage capacity (Aryana and Kovscek, 2012; Guo and Aryana, 2019; Wang et al., 2023). The significance of accurate estimations of the thermophysical properties of H_2 extends to underground hydrogen storage in salt caverns (Liu et al., 2022a). Hematpur et al. (2023) pointed out that knowing the thermal conductivity of H_2 is crucial as it directly informs increases in pressure and temperature during storage operations.

Furthermore, integrating thermodynamic models into simulation platforms is critical to developing robust simulation frameworks (Wang and Aryana, 2021; Liu et al., 2022b). Such frameworks are essential for accurately characterizing the behavior of working fluids across various industrial processes and systems, including production, transportation, compression, and storage. Applying principles of thermodynamics and fluid dynamics within these simulations makes it possible to predict and analyze the behavior of fluids under varying conditions of pressure, temperature, and volume with greater precision. Given its predominantly gaseous state under ambient conditions, a deep understanding of its mixed-state properties is essential for designing efficient storage and distribution systems. In navigating the complexities of H_2-based technologies, empirical correlations are invaluable tools, providing a reliable method to compute system properties (Jaeschke and Humphreys, 1991). This paper reviews existing data and evaluates established models in this research area. The compiled dataset forms the foundational bedrock for crucial H_2 property estimations. Moreover, these correlations have been validated across a range of properties, including isothermal compressibility, volume expansion, fugacity coefficient, enthalpy, entropy, Helmholtz energy, Gibbs energy, adiabatic bulk modulus, speed of sound, as well as kinematic viscosity and thermal diffusivity.

2. Review of literature-based data

H_2 is the lightest diatomic molecule, with a molecular weight of approximately two atomic mass units and a bond length of about 0.74 angstroms, placing it among the smallest molecules (Elliott et al., 2023). The critical properties and acentric factors of CO_2, CH_4, and H_2 are presented in Table 1.

Considering the principles of the corresponding states, this table highlights the distinct differences between H_2, CO_2, and CH_4. It underscores how unique the properties of H_2 are, especially when compared to CH_4 and CO_2. This work presents data for pure hydrogen, comprising 3,396 data points for density (ρ), 939 data points for viscosity (μ), and 2,287 data points for thermal conductivity (λ). The density data range from 0.040 to 762.195 mole/L, with temperatures varying from 100.03 to 926.7 K and pressures ranging from atmospheric to 1.9835 GPa. The viscosity data cover temperatures from 100 to 1,100 K and atmospheric to 217 MPa pressures, with viscosity values between 4.134×10^{-6} and 2.26×10^{-5} Pa·s. The thermal conductivity data lie between 0.0691 and 0.4627 W/(m·K), with temperatures ranging from 98 to 1,000 K and pressures from atmospheric to 99 MPa. Admittedly, different sources of experimental data exist for the thermophysical properties of H_2. Nevertheless, the uncertainty of data sets varies (Cheng et al., 2021; Li et al., 2023b); in this study, REFPROP10 (Lemmon et al., 2018) predictions are used to select reference literature data for the analysis.

The density data are sourced from eighteen literature references, with the earliest data dating back to 1893. The viscosity data have been collected from twenty-nine sources, with the earliest data available from 1930. Similarly, the thermal conductivity data have been collected from fourteen sources, with the earliest data available from 1970. This extensive

Table 2. Summary of collected density data.

References	NDP	T (K)	p (MPa)	ρ (mole/L)
Cheng et al. (2020)	21	723.30-926.70	5.741-6.258	0.805-0.942
Sakoda et al. (2012)	104	353.22-473.19	1.072-99.849	0.305-22.045
Jaeschke and Humphreys (1991) Gasunie	68	273.15-353.13	0.210-26.265	0.087-9.796
Jaeschke and Humphreys (1991) Ruhrgas	221	273.15-353.13	0.497-28.125	0.190-10.392
Liebenberg et al. (1978)	13	100.81-163.91	776.4-1871	75.872-91.827
Liebenberg et al. (1977)	1,747	100.81-307.39	206.1-1,983.5	37.092-762.195
Presnall (1969)	108	473.1-873.03	10.132-182.385	1.540-27.041
Michels et al. (1959)	465	103.17-423.13	0.571-299.161	0.350-43.060
Johnston et al. (1953)	58	100.03-299.96	1.765-20.480	0.865-19.553
Michels and Goudeket (1941)	283	273.15-423.13	0.929-300.936	0.406-41.869
Wiebe and Gaddy (1938)	47	273.15-573.18	2.533-101.325	0.806-26.095
Townend and Bhatt (1931)	40	273.15-298.13	0.101-60.795	0.041-18.862
Bartlett et al. (1930)	37	203.19-293.13	2.566-102.667	1.492-31.272
Scott (1929)	18	298.13	0.101-17.225	0.040-6.303
Bartlett et al. (1928)	43	273.15-672.63	5.0662-101.325	1.260-26.063
Bartlett (1927)	8	273.15	5.0662-101.325	2.157-26.001
Verschoyle (1926)	25	273.15-293.14	4.672-20.820	1.865-8.075
Holborn and Otto (1925)	17	123.14-223.26	2.165-10.018	1.150-9.124
Amagat (1893)	73	273.15-320.43	0.101-303.975	0.044-44.036
Total	3,396	100.03-926.7	0.101-1,983.5	0.040-762.195

Notes: NDP: number of data points.

temporal coverage underscores the depth and thoroughness of our review, offering a broad perspective on the evolution and refinement of H_2 thermophysical measurements over the years. Details of the collected density, viscosity, and thermal conductivity data are listed in Tables 2, 3, and 4.

2.1 Density

Table 2 provides a comprehensive listing of the sources for H_2 density data. The compilation spans a significant timeframe, capturing published data that extends from as early as 1893 through to 2020.

The primary contributions to this collection stem from studies conducted by Michels and Goudeket (1941), Michels et al. (1959), and Liebenberg et al. (1977). Within the temperature range considered for this study, H_2 behaves as an ideal gas at pressures below 1 MPa. However, at pressures exceeding 1 GPa, data sources become sparse. The highest reported temperature is 926.7 K. Table 1 and Fig. 1 show that data span temperatures from 273 to 473 K up to 100 MPa, but datasets for higher temperatures remain limited.

2.2 Viscosity

In total, 939 viscosity data points have been collected from open literature. The compiled dataset includes 170 data points

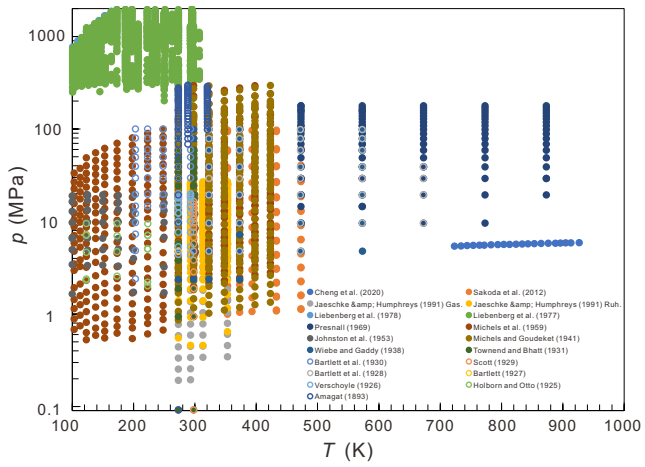

Fig. 1. Temperature-pressure distribution of collected density data.

at pressures below atmospheric, which can be considered as representing dilute/zero density gas viscosity (Hanley et al., 1970). The remaining 769 data points are measured at higher pressures. The temperature range for the dilute viscosity measurements spans from 100 to 1,000 K, with corresponding viscosity values ranging from 4.134×10^{-6} to 2.088×10^{-5} Pa·s.

Table 3. Summary of collected viscosity data.

References	NDP	T (K)	p (MPa)	μ ($\times 10^6$ Pa·s)
Sakoda et al. (2015)†	20	296.26-573.48	0.099-0.702	8.9-14.27
Song et al. (2013)†	22	298-1,000	0	8.8394-20.861
Muzny et al. (2013)	111	225-400	0.295-3.399	7.36-10.91
Yusibani et al. (2011)	17	294.52-400.12	4.69-99.33	9.01-12.84
Mehl et al. (2010)†	14	100-1,000	0	4.134-20.88
May et al. (2007)†	32	213.61-394.21	0-0.1	7.07-10.805
Mal'tsev et al. (2004)	3	500-1,100	0.3	12.9-17.9
Nabizadeh and Mayinger (1999)†	76	295.55-399.15	0.098-5.775	8.908-11.131
Lukin et al. (1983)†	20	103.21-293.2	0.101325	4.33-8.79
Clifford et al. (1981)†	2	298.14-308.14	0.1	8.925-9.122
Chuang et al. (1976)	36	173.16-273.15	0.404-50.587	6.071-9.825
Carey et al. (1974)	18	269.31-299.19	0.1455-10.988	8.82-9.12
Kestin et al. (1971)†	3	295.48-308.40	0.103-0.106	8.851-9.131
Hanley et al. (1970)†	14	100-1,000	0	4.179-20.298
Golubev and Petrov (1966)†	58	288.15-523.11	0.101-81.06	8.66-14
Gracki et al. (1969)	42	173.16-298.14	0.462-17.134	6.147-9.141
Rudenko and Sliusar (1968)†	65	100.02-299.98	0.101-217.139	5.6-16.5
Kestin and Yata (1968)	11	293.15-303.15	0.106-2.389	8.825-9.039
Golubev and Shepeleva (1966)	53	144.66-273.15	0.981-49.13	5.49-9.975
Tsederberg et al. (1965)	28	288.64-990.35	4.35-50.55	8.71-20.26
Diller (1965)	11	100	1.506-35.836	4.32-8.45
Menabde (1965)†	9	111.06-299.63	0.006	4.53-9.02
Barua et al. (1964)	38	223.19-423.13	1.019-17.783	7.281-11.505
Kestin and Nagashima (1964)†	26	293.13-303.13	0-23.973	8.825-9.043
Kestin and Wang (1958)	10	298.13	0.101-7.09	8.923-9.063
Michels et al. (1953)	95	298.13-398.13	2.592-186.258	8.941-16.02
Kuss (1952)†	27	298.13-348.12	0.098-49.033	8.9-10.87
Johnston and McCloskey (1940)†	23	117.48-300.03	0.020-0.100	4.741-8.96
Boyd Jr (1930)	56	303.15-343.15	7.214-19.424	9.08-11.68
Total	940	100-1,100	0-217.1394	4.134-22.6

Notes: † Includes data for dilute or zero-density gas viscosity.

Table 3 lists the viscosity data for pure H_2. Sources that provide dilute/zero-density gas viscosity data are indicated with a dagger (†). Fig. 2 illustrates the temperature-pressure distribution for the viscosity of dense pure H_2 based on the collected data. A noticeable scarcity of data exists for temperatures exceeding 525 K and pressures beyond 80 MPa, as reflected in Fig. 2. Conversely, data for temperatures under 400 K and pressures up to 60 MPa are well-represented.

2.3 Thermal conductivity

For thermal conductivity, a total of 2,287 data points have been collected. Of these, 41 data points are measured at pressures below atmospheric and can be classified as dilute/zero density gas thermal conductivity (Hanley et al., 1970), while the remaining data points pertain to dense pure H_2, as detailed in Table 4. Sources providing dilute/zero-density gas thermal conductivity data are denoted with a dagger.

Fig. 3 delineates the distribution of thermal conductivity data for pure H_2 within a temperature-pressure parameter space. There is a noticeable data scarcity in regions with tem-

Table 4. Summary of collected thermal conductivity data.

References	NDP	T (K)	p (MPa)	λ (W/(m·K))
Song et al. (2013)†	22	298-2000	0	0.1858-0.8808
Moroe et al. (2011)	198	323.19-771.92	0.261-99.205	0.197-0.4188
Assael et al. (2011) HW*	279	300.88-600.43	0.291-22.629	0.1842-0.3115
Assael et al. (2011) THW**	525	301.17-601.18	1.980-70.096	0.1889-0.3386
Hemminger (1987)†	6	313.14-463.11	0.1	0.1935-0.2568
Mustafa et al. (1987)	51	307.8-428.83	1.98-9.89	0.1954-0.2517
Roder (1984)	1,054	98.63-315.33	0.424-69.746	0.0704-0.2509
Clifford and Platts (1981)	41	310.57-384.62	1.9-23.47	0.1947-0.2374
Assael and Wakeham (1981)	12	307.10-307.64	2-9.17	0.19356-0.19825
Clifford and Platts (1981)	30	300.05-301.44	2.1-36.13	0.1909-0.2175
Clerc et al. (1977)†	16	298.14-373.12	0.1-60	0.183-0.2504
Clifford et al. (1975)†	1	283.12	0.101325	0.1779
Leneindre (1972)†	28	273.15-873.03	0.1-80	0.1695-0.4077
Roder and Diller (1970)	24	99.83-198.05	0.132-9.829	0.0691-0.1488
Total	2,287	98.63-1,000	0-99.205	0.0691-0.46269

Notes: HW*: hot wire; THW**: transient hot wire; †Includes data for dilute or zero-density gas thermal conductivity.

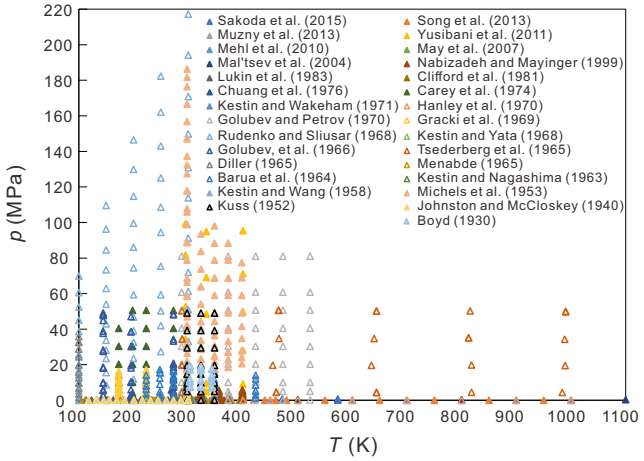

Fig. 2. Distribution of viscosity data with respect to temperature and pressure.

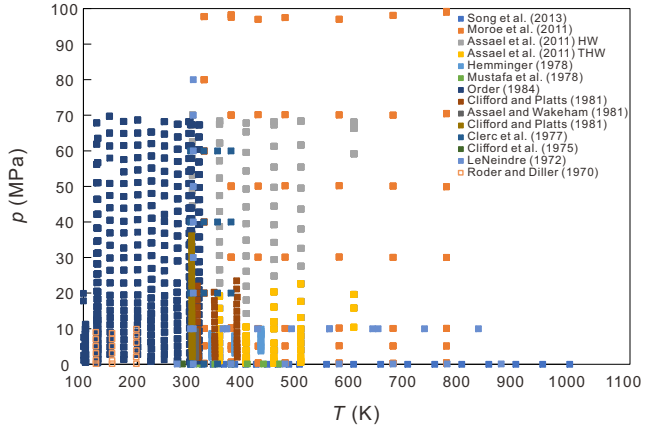

Fig. 3. Temperature-pressure distribution of the dense thermal conductivity collected data.

peratures above 500 K and pressures exceeding 70 MPa. Conversely, the dataset appears more comprehensive for conditions characterized by temperatures and pressures that fall below these thresholds. This more populated region suggests that most experimental studies have focused on these more moderate temperature and pressure conditions.

For any model development and parameter determination, ensuring the reliability of the experimental data is key. The Reference Fluid Thermodynamic and Transport Properties REFPROP10 (Lemmon et al., 2018) database, developed by the National Institute of Standards and Technology, provides a comprehensive collection of thermodynamic and transport properties for various fluids, encompassing pure substances and mixtures. This resource serves as a benchmark for accurate and reliable data. Using the methodologies outlined in Eqs. (1)-(3), the collected data are assessed against REFPROP10 (Lemmon et al., 2018), reporting metrics such as the absolute average deviation (AAD), the coefficient of determination (R^2), and the percentage of accuracy-precision (PAP) (Heidaryan, 2019):

$$\mathrm{AAD}\% = \frac{100}{\mathrm{NDP}} \sum_{i=1}^{\mathrm{NDP}} \left| \frac{X_i^{\mathrm{exp.}} - X_i^{\mathrm{calc.}}}{X_i^{\mathrm{exp.}}} \right| \tag{1}$$

$$R^2 = \left(\frac{NDP \sum_{i=1}^{NDP} \left(X^{exp.} X^{calc.}\right) - \sum_{i=1}^{NDP} X^{exp.} \sum_{i=1}^{NDP} X^{calc.}}{\sqrt{\left(NDP \sum_{i=1}^{NDP} (X^{exp.})^2 - \left(\sum_{i=1}^{NDP} X^{exp.}\right)^2\right)\left(NDP \sum_{i=1}^{NDP} (X^{calc.})^2 - \left(\sum_{i=1}^{NDP} X^{calc.}\right)^2\right)}} \right)^2 \quad (2)$$

$$PAP = 100\left(1 - \frac{\sqrt{2}}{2}\sqrt{\left(\left(\frac{\sum_{i=1}^{NDP}\left|\frac{X_i^{exp.} - X_i^{calc.}}{X_i^{exp}}\right|}{NDP}\right)^2 + \left(\frac{\sum_{i=1}^{NDP}(X^{exp.} - X^{calc.})^2}{\sum_{i=1}^{NDP}(X^{exp.} - \bar{X}^{exp.})^2}\right)^2\right)}\right) \quad (3)$$

where NDP is the number of data points, $X_i^{exp.}$ is each individual data point obtained experimentally, and $X_i^{calc.}$ is the corresponding calculated value. The maximum absolute deviation (MaxAD) indicates the maximum estimation deviations. Table 5 presents a comprehensive breakdown of statistical metrics for each data set. These metrics provide insights into the accuracy and precision of the collected data from various literature sources, allowing for an informed assessment of their quality and consistency.

Table 5. Statistical metrics of collected experimental data versus REFPROP 10 (Lemmon et al., 2018).

Properties	AAD%	MaxAD%	R^2	PAP
ρ	0.5843	6.343	0.9995	99.584
μ	1.2344	16.47	0.9943	99.026
λ	1.1847	7.25	0.9974	99.162

3. Development of correlations

3.1 Compressibility factor (density)

Bridgman (1924) made a notable contribution to thermophysical modeling by proposing an equation of state (EoS) specifically for gaseous hydrogen. This EoS signifies one of the first attempts to capture the volumetric properties of hydrogen within a mathematical framework. Tracing back further into the annals of empirical research, attempts to represent the volumetric behavior of H_2 can be dated as early as 1912. During this period, Haas and Onnes (1912) meticulously investigated virial coefficients, providing foundational insights into hydrogen's behavior across various temperatures. In the subsequent years following these seminal works, the scientific community has been actively devising and refining mathematical models. These efforts, aimed at estimating and comprehending the thermodynamic properties of hydrogen, have culminated in many models, as documented in various references (Mills et al., 1977; Spycher and Reed, 1988; Tkacz and Litwiniuk, 2002; Lemmon et al., 2006; Lemmon et al., 2008; Joubert, 2010; Davarnejad et al., 2014; Striednig et al., 2014; De Lucia et al., 2015; Zheng et al., 2016; Sezgin et al., 2017; Park and Chae, 2022; Wei et al., 2023).

Drawing inspiration from statistical mechanics, the number of interacting particles correlates with the multiparticle interactions at each gas density, especially for high-temperature gases (Reed and Gubbins, 1973). Consequently, given the elevated temperatures, it's logical to represent Z, the compressibility factor, defined as $Z \equiv p/(\rho RT)$, where R is 8.314472 J/(mole·K) as a function of $p^{1/3}$ and 1/T using a series of polynomials (as illustrated in Fig. 4). However, in this work, the relationship is empirically modified as:

$$Z = 1 - \frac{a_1 p^{\frac{1}{3}}}{T^{a_2}} - \frac{a_3 p^{\frac{2}{3}}}{T} + \frac{a_4 p}{T} - \frac{a_5 p^{a_6}}{T} \quad (4)$$

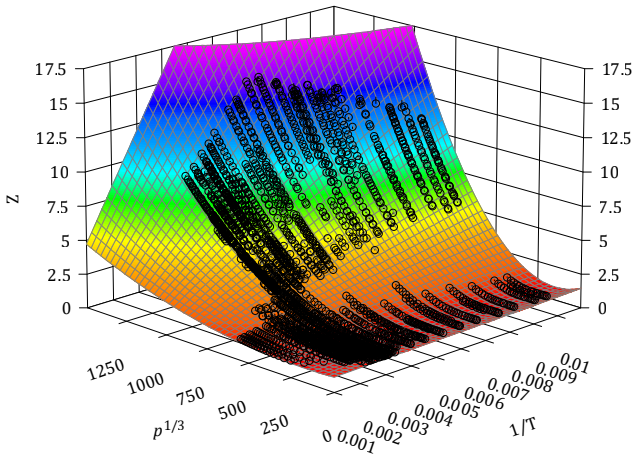

Fig. 4. Plot of experimental Z against a polynomial function of $p^{1/3}$ and $1/T$.

where, T is the temperature in K, p is the pressure in Pa, the constants a_1 through a_6 are fitting parameters whose values are listed in Table 6. Eq. (4) offers a straightforward relation for reliably estimating the H_2 compressibility factor (Z-factor), concurrently highlighting the deviations from an ideal gas.

Figs. 5 and 6 visually represent the inaccuracies associated with calculating the Z-factor, mapped against temperature and pressure, respectively. Notably, when observing the temperature-driven discrepancies, the Z-factor calculation becomes error-prone below 300 K, with deviations sometimes surpassing two percent. This suggests a certain instability or variability in the Z-factor at these cooler temperatures. Conversely, the calculations stabilize at temperatures larger than 300 K, with deviations predominantly clustering around the one percent mark. This relative stability at increased temperatures highlights the importance of understanding the

Table 6. Parameters derived from the fitting of the correlations.

i	a_i (Eq. (4))	b_i (Eq. (5))	c_i (Eq. (6))	d_i (Eq. (7))	e_i (Eqs. (8) and (9))
1	2.39373421×10^{1}	$1.81758329 \times 10^{-7}$	$2.34498695 \times 10^{-3}$	2.14987264×10^{1}	2.97625611×10^{3}
2	2.48175737×10^{0}	$6.83106758 \times 10^{-1}$	$7.64814482 \times 10^{-1}$	9.19000043×10^{0}	$2.45206944 \times 10^{-2}$
3	$2.25819778 \times 10^{-4}$	$9.32706091 \times 10^{-13}$	$1.39412767 \times 10^{-8}$	8.8333041×10^{2}	2.75669411×10^{0}
4	$3.46012447 \times 10^{-6}$	1.48078541×10^{0}	$8.51102621 \times 10^{-1}$	1.50776686×10^{1}	/
5	$1.44207517 \times 10^{-8}$	1.27555239×10^{0}	1.11721850×10^{0}	3.17983480×10^{2}	/
6	1.23194905×10^{0}	/	/	/	/

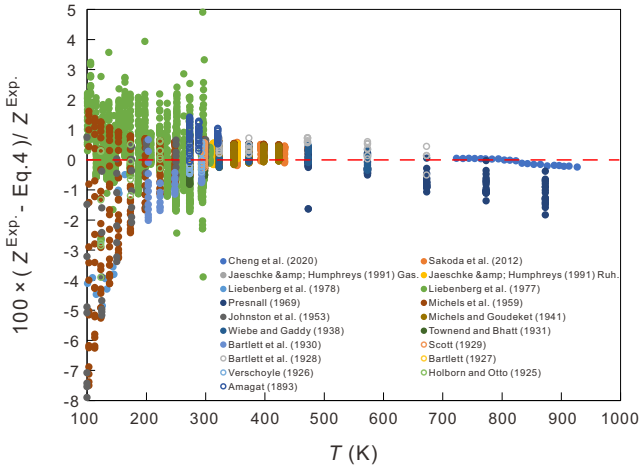

Fig. 5. Deviation in the compressibility factor determined using Eq. (4), plotted against experimental temperature.

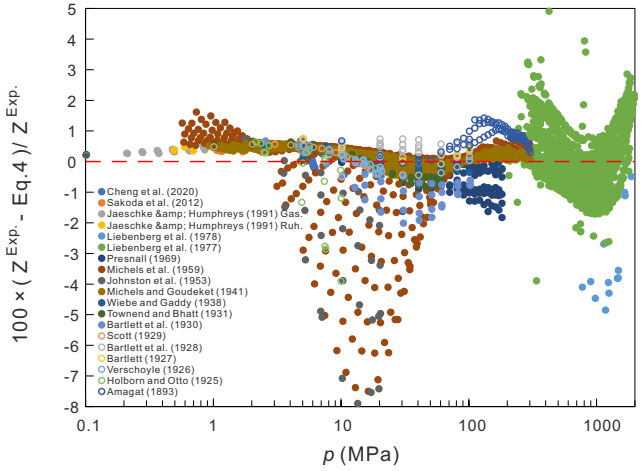

Fig. 6. Deviation in the compressibility factor determined using Eq. (4), plotted against experimental pressure.

temperature dependencies when working with the Z-factor in hydrogen-related applications.

From the standpoint of pressure considerations, the most pronounced deviations appear at pressures larger than 200 MPa. Deviations exceeding two percent can be traced back to two sets of experimental observations for pressures that fall below 200 MPa. This indicates that most data are consistent, but these two sets stand out. However, even when considering these anomalies, the calculated deviation never exceeds ten percent, which is a testament to the robustness and reliability of Eq. (4) for determining the compressibility factor of hydrogen under various conditions. This suggests that, while there are minor discrepancies in specific data regions, the overall mathematical model provides a reasonably accurate representation across a broad spectrum of conditions.

3.2 Viscosity

Viscosity is a crucial thermophysical property that quantifies a fluid's inherent resistance to shear flow, effectively depicting its internal frictional interactions at the molecular level (Millat et al., 1996). This parameter is paramount for understanding flow dynamics and designing engineering systems. H_2 exhibits a notably low viscosity, which can be attributed to its small molecular size and the inherent properties of diatomic gases. This low-viscosity characteristic of H_2 is special significance in many engineering and industrial applications. When hydrogen serves as the primary fluid, its ease of flow facilitates efficient mass and heat transfer in various systems. This is especially pronounced in flow conduits such as ducts, pipes, and heat exchangers, where reduced frictional resistance can lead to energy savings and enhanced system performance.

Beyond heuristic approaches (Park and Chae, 2022), the modeling of H_2 viscosity predominantly relies on the free volume theory (Jossi et al., 1962; Diller, 1965; McCarty, 1972; Yusibani et al., 2011; Muzny et al., 2013). The foundational structure of these models is consistent across studies. Specifically, the total viscosity of a pure fluid is represented as the sum of the viscosity of H_2 at the zero-density limit (Assael et al., 1986) and an additional residual component. The viscosity of H_2 is characteristically low within the scope and range examined in this study. This specific behavior lends itself to representation through a power law expression as:

$$\mu = b_1 T^{b_2} + b_3 T^{-b_4} p^{b_5} \tag{5}$$

where μ is the viscosity in Pa·s. The constants b_1 through b_5 are fitting parameters whose values are listed in Table 6. The cross plot shown in Fig. 7 demonstrates the reliability of Eq. (5) in estimating the viscosity of pure H_2. Upon closer analysis, it becomes clear that significant deviations predominantly originate from the data sets provided by Boyd Jr (1930), which is the most antiquated in the collection, and that by Gracki et al. (1969). Despite these anomalies, most

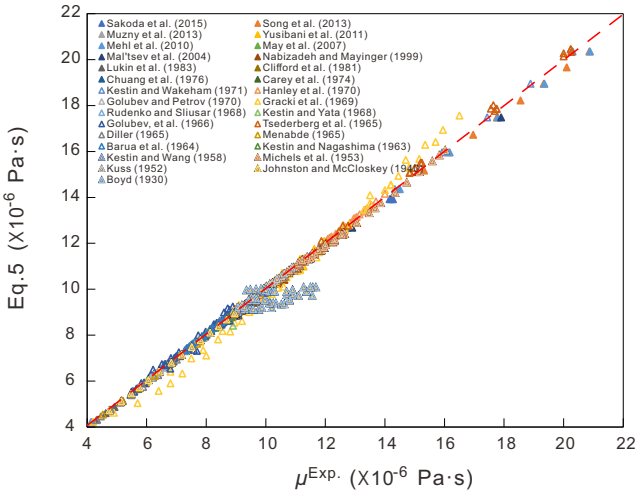

Fig. 7. Illustration of the efficacy of Eq. (5) in estimating the viscosity of H_2.

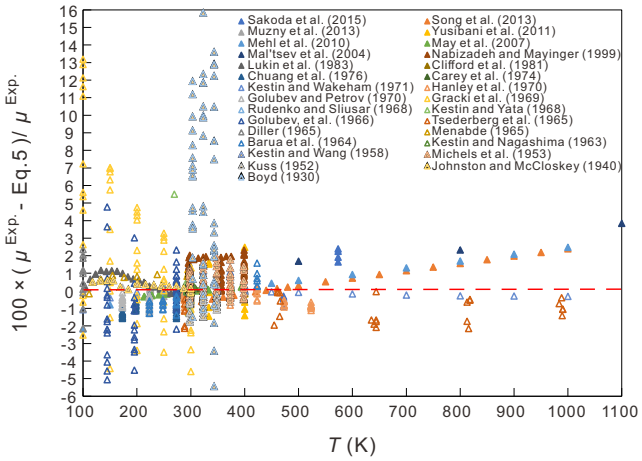

Fig. 8. Deviation in estimating H_2 viscosity as a function of temperature using Eq. (5).

data sets correlate with the proposed equation, underscoring its potential applicability in many contexts. Figs. 8 and 9 visually represent the deviation in viscosity calculations, with Fig. 8 focusing on temperature dependence and Fig. 9 on pressure dependence. When closely examining these charts, one can observe that by setting aside the data from Boyd Jr (1930) and Gracki et al. (1969), most deviations in viscosity calculations remain within a two percent boundary. This consistency in deviation suggests a high degree of reliability in our measurements. Furthermore, this consistent error margin of approximately two percent further underscores the validity and robustness of the formulated viscosity correlation, Eq. (5), making it a valuable tool for accurately estimating the viscosity of H_2 in various conditions.

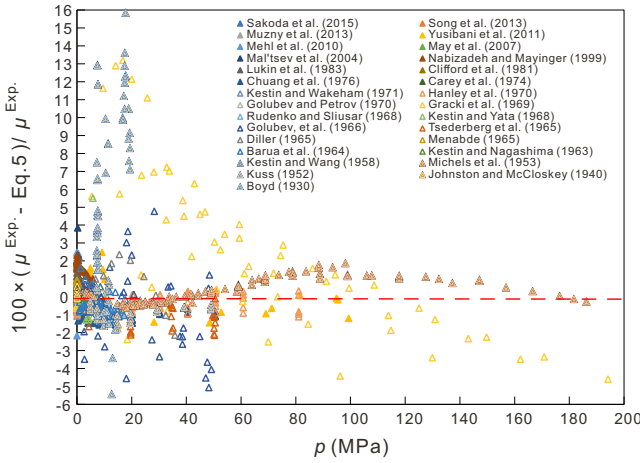

Fig. 9. Variability in predicting H_2 viscosity based on pressure using Eq. (5).

3.3 Thermal conductivity

The low viscosity and high thermal conductivity enable H_2 to facilitate rapid and efficient heat transfer. It is an ideal medium for many applications, especially in high-tech industries where effective heat management is important (Assael and Wakeham, 1981). Analogous to the transition away from heuristic methods in viscosity modeling (Park and Chae, 2022), the representation of H_2 thermal conductivity is chiefly anchored in the free volume theory (Stiel and Thodos, 1964; Roder, 1984; Assael et al., 2011; Moroe et al., 2011). Essentially, the thermal conductivity of H_2 is modeled following the same principles as its viscosity. However, a similar approach can be used here when dealing with thermal conductivity data. This procedure can be described as:

$$\lambda = c_1 T^{c_2} + c_3 T^{-c_4} p^{c_5} \tag{6}$$

where λ is the thermal conductivity in W/(m · K), and c_1 through c_5 are fitting parameters whose values are listed in Table 4. Fig. 12 shows that Eq. (4) reliably estimates the thermal conductivity of pure high-pressure H_2.

The cross plot presented in Fig. 10 demonstrates the reliability of Eq. (6) for estimating the thermal conductivity of pure H_2. Upon closer examination, it is evident that significant

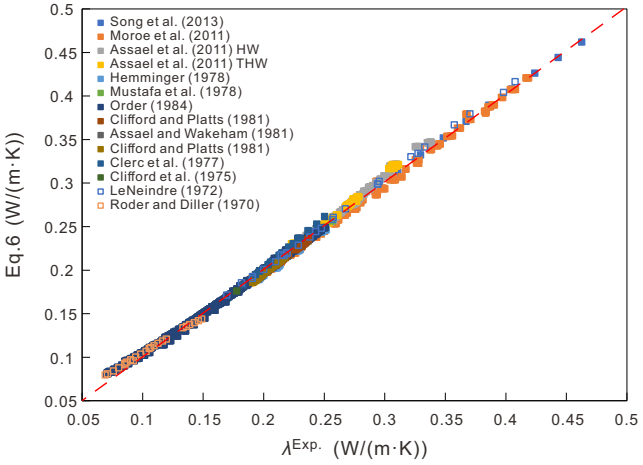

Fig. 10. Reliability of Eq. (6) in estimating pure H_2 experimental thermal conductivity.

overestimation primarily arises from the data sets provided by Roder and Diller (1970), the oldest dataset in the collection, which falls within the lower portion of collected data (0.1 to

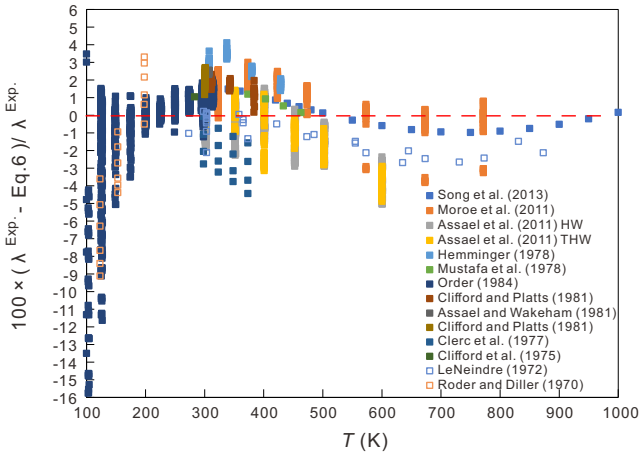

Fig. 11. Deviation of Eq. (6) in calculations of H_2 thermal conductivity as a function of temperature.

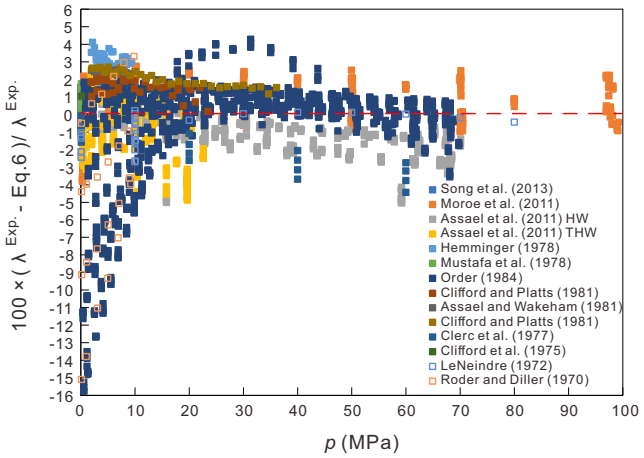

Fig. 12. Deviation of Eq. (6) in calculations of H_2 thermal conductivity as a function of pressure.

0.15 W/(m·K). Despite these outliers, most data sets align well with the proposed equation, highlighting its potential relevance in various contexts.

Figs. 11 and 12 display the estimation errors for thermal conductivity as functions of temperature and pressure, respectively. These Figures show that the data from Roder and Diller (1970) and Roder (1984) deviate from other data sets. The primary deviation occurs at temperatures below 200 K and pressures below 10 MPa. Based on the representation in these Figures, the error associated with thermal conductivity calculations is typically under five percent. Thus, it can be inferred that the correlation presented in Eq. (6) offers a reliable method for estimating the thermal conductivity of dense H_2.

3.4 Ideal gas isobaric heat capacity

The optimization of chemical processes is a sophisticated undertaking that plays a pivotal role in enhancing efficiency and conserving resources. Central to this optimization is the accurate calculation of energy requirements. To accurately gauge these requirements, two fundamental parameters need to be determined: the enthalpy change, which provides insights

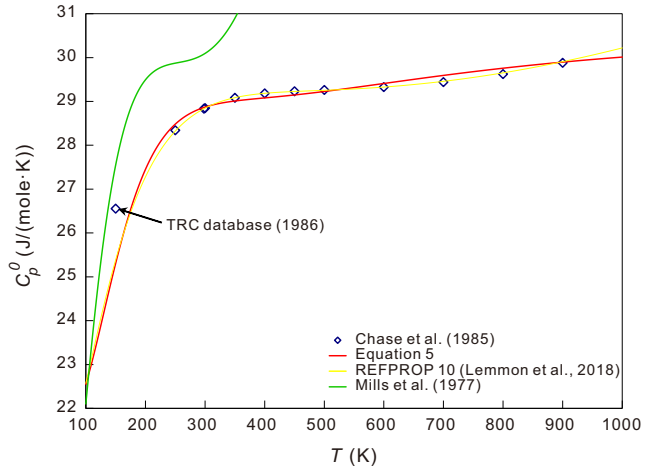

Fig. 13. Ideal gas isobaric heat capacity of H_2 as a function of temperature.

into the heat transfer associated with a reaction or phase transition, and the isobaric heat capacity, which indicates the amount of heat required to change the temperature of a substance at constant pressure (Jarrahian et al., 2014). Together, these parameters offer valuable information to refine and improve the performance of various chemical processes. As discussed by Bartolomeu and Franco (2020), the isobaric heat capacity of H_2 above 100 K is dominated by the ideal gas heat capacity. The ideal gas isobaric heat capacity of H_2 (C_p^0), can be correlated using the equation proposed by Aly and Lee (1981), as:

$$C_p^0 = d_1 + d_2\left(\frac{\frac{d_3}{T}}{\sinh\frac{d_3}{T}}\right)^2 + d_4\left(\frac{\frac{d_5}{T}}{\cosh\frac{d_5}{T}}\right)^2 \tag{7}$$

where d_1 through d_5 are fitting parameters. Eq. (7) is meticulously fitted to data from the work of Chase et al. (1985), and its parameters are provided in Table 6. Fig. 13 shows the performance of Eq. (7) in estimating the isobaric heat capacity of H_2 when treated as an ideal gas. This representation is juxtaposed against results from REFPROP 10 (Lemmon et al., 2018) and the correlation proposed by Mills et al. (1977). In Fig. 13, the data point at 150 K is sourced directly from the TRC (1986). The equation proposed by Aly and Lee (1981) can be used to calculate both the ideal gas enthalpy (H^0) as:

$$H^0 = d_1 T + d_2 T\left(\frac{d_3}{T}\right)\coth\frac{d_3}{T} - d_4 T\left(\frac{d_5}{T}\right)\tanh\frac{d_5}{T} + e_1 \tag{8}$$

and the ideal gas entropy (S^0) as:

$$S^0 = d_1\ln T + d_2\left(\left(\frac{d_3}{T}\right)\coth\left(\frac{d_3}{T}\right) - \ln\left(\sinh\left(\frac{d_3}{T}\right)\right)\right) - d_4\left(\left(\frac{d_5}{T}\right)\tanh\left(\frac{d_5}{T}\right) - \ln\left(\cosh\left(\frac{d_5}{T}\right)\right)\right) - e_2\ln^{e_3}(p) \tag{9}$$

where e_1 through e_3 are fitting parameters. These calculations adhere to the definitions provided by Smith et al. (2022). The constants e_1 to e_3 were determined through a fitting using data from Lemmon et al. (2018). In Eqs (7)-(9), T is expressed in

Table 7. Statistical metrics for various methods used in estimating H_2 density.

References	NOC	AAD%	MaxAD%	R^2	PAP
REFPROP 10 (Lemmon et al., 2018)*	60	0.5843	6.343	0.9995	99.584
Eq. (4)	6	0.633	7.897	0.9998	99.552
Tkacz and Litwiniuk (2002)	5	0.723	5.394	0.9998	99.488
Joubert (2010)	11	1.089	12.69	0.9998	99.226
Sezgin et al. (2017)	2	2.385	12.17	0.9988	98.284
Mills et al. (1977)	9	2.604	28.18	0.9997	98.158
Spycher and Reed (1988)	6	11.42	131.2	0.9111	47.059
Chen et al. (2010)	1	12.19	52.93	0.9884	81.046
De Lucia et al. (2015)	6	44.6475	97.48	0.6981	2.687
Wei et al. (2023)	17	54.7714	233.8	0.9414	Null
Park and Chae (2022)	21	73.7724	20,679	0.0009	Null
Striednig et al. (2014)	6	279.3808	2,346.2	0.7589	Null
Lemmon et al. (2008)	27	44,402.52	1,687,354	0.3428	Null
Davarnejad et al. (2014)	55	120,434.6	824,631	0.5888	Null
Zheng et al. (2016)	24	259,205.1	9,210,476	0.3469	Null
Lemmon et al. (2006)	16	923,339.2	29,781,436	0.389	Null
Zheng et al. (2016)	45	3.85×10^9	2.25×10^{11}	0.1575	Null

Notes: NOC: Number of constants; *REFPROP 10 employs the EoS developed by Leachman et al. (2009).

K, p is in Pa, C_p^0 and S^0 are in J/(mole· K), and H^0 is in J/mole. A dimensional analysis of the constants highlighted in Table 6 reveals that they are not dimensionless. This is due to the empirical basis of these equations, which makes it challenging to draw a direct link between the parameters and the inherent characteristics of H_2. Given this context, and to avoid potential misconceptions, the dimensions associated with the constants have been intentionally omitted from the table.

4. Results and discussion

This work compares predicted outcomes to observed data, details deviation margins, and analyzes the goodness of fit in regression analysis. Such a comprehensive approach ensures the model's reliability and robustness in diverse scenarios. Statistical parameters that have been introduced in Eqs. (1)-(3) are used to calculate parameters for different proposed equations. Table 7 lists the statistical metrics for various explicit methods designed to estimate the density of H_2, benchmarking them against REFPROP 10 (Lemmon et al., 2018).

Notably, Eq. (4), Tkacz and Litwiniuk (2002), and Joubert (2010) stand out as reliable approaches (PAP>99) for estimating gaseous H_2 density. This observation, however, does not imply that other methods are inherently inferior. It is worth noting that many of these alternative methods were crafted for specific, narrow temperature and pressure ranges. In their development, added parameters were introduced to enhance the accuracy and precision of the respective equations. This tailored approach occasionally leads to deviations when extrapolating beyond their intended domain. Consequently, it is advisable to utilize these methods judiciously.

Table 8 provides a detailed analysis of the statistical metrics used by various methods formulated to estimate the viscosity of H_2, using REFPROP 10 (Lemmon et al., 2018) as a benchmark. With the exceptions of Eq. (5) and the correlation developed by Park and Chae (2022), which utilize both pressure and temperature as inputs, the remaining models are grounded in the Free Volume Theory and require density as an input. For a consistent evaluation across all methods, densities were computed using REFPROP 10 (Lemmon et al., 2018).

Apart from the correlation developed by Park and Chae (2022), the statistical metrics listed in Table 8 were calculated based on model estimates within their intended domain. The extension by McCarty (1972) of the method proposed by Diller (1965) does not yield significant improvements. Although the correlation developed by Muzny et al. (2013) ranks as the top performer in terms of PAP, Eq. (5) demonstrates the lowest values in terms of AAD% and MaxAD%. PAP scores below 90 suggest an inconsistency in the model's ability to produce results within the acceptable range.

Table 9 compares various methods and their effectiveness in estimating the thermal conductivity of H_2, with the top entries showing better reliability than the methods listed toward the bottom.

While Eq. (6) demonstrates commendable reliability, the

Table 8. Statistical metrics for various methods used in estimating H_2 viscosity.

References	NOC	AAD%	MaxAD%	R^2	PAP
REFPROP 10 (Lemmon et al., 2018)*	18	1.234	16.471	0.994	99.026
Eq. (5)	5	1.206	15.835	0.990	98.891
Wei et al. (2023)	12	2.311	44.274	0.916	93.312
McCarty (1972)	24	6.26	70.355	0.709	72.858
Diller (1965)	22	6.26	70.355	0.709	72.858
Yusibani et al. (2011)	20	6.764	70.607	0.71	71.955
Jossi et al. (1962)	10	55.868	1,068.996	0.177	Null
Park and Chae (2022)	21	25.255	2,828.709	0.22	Null

Notes: NOC: Number of constants; *REFPROP 10 in the correlation developed by Muzny et al. (2013).

Table 9. Statistical metrics for various methods used in estimating H_2 thermal conductivity.

References	NOC	AAD%	MaxAD%	R^2	PAP
REFPROP 10 (Lemmon et al., 2018)*	20	1.185	7.2471	0.9974	99.16
Eq. (6)	5	1.648	15.765	0.9959	99.21
Moroe et al. (2011)	27	2.560	9.9482	0.9958	98.19
Stiel and Thodos (1964)**	8	4.167	27.730	0.9825	97.04
Roder (1984)**	10	124.65	16,684.1	0.0115	Null
Park and Chae (2022)	21	207.31	36,638.5	0.1269	Null

Notes: NOC: Number of constants; *REFPROP 10 employs the correlation developed by Assael et al. (2011); ** The thermal conductivity at zero density was calculated using the correlation developed by Assael et al. (1986).

method proposed by Moroe et al. (2011) also exhibits a respectable balance between AAD% and R^2. However, it is important to approach the results of Stiel and Thodos (1964) cautiously due to the observed increase in their AAD% values. Models developed by Roder (1984) and Park and Chae (2022) present substantial deviations, as demonstrated in the elevated AAD% and MaxAD% and decreased R^2 and PAP values. While these methods offer valuable insights, they may be context specific.

Derived properties can be calculated from these correlations, acknowledging the interconnected nature of these parameters. As previously mentioned, REFPROP 10 (Lemmon et al., 2018) offers an extensive database of thermodynamic and transport properties for various fluids, encompassing pure substances and mixtures. To illustrate the efficacy of the developed equations, eighty-six isotherms account for 8,600 data points generated by REFPROP 10 (Lemmon et al., 2018) within the temperature range of 150-1,000 K and pressures between 0.1 and 100 MPa. The statistical metrics comparing the proposed correlations with these 8,600 data points from REFPROP 10 (Lemmon et al., 2018) can be found in Table 10.

4.1 Isothermal compressibility coefficient

The isothermal compressibility coefficient (κ_T) measures how a substance's volume changes in response to pressure variations at constant temperature. Using Eq. (4), this relationship can be expressed as:

$$\kappa_T = \frac{1}{p} - \frac{\left(\frac{\partial Z}{\partial p}\right)_T}{Z} \tag{10}$$

where

$$\left(\frac{\partial Z}{\partial p}\right)_T = -\frac{a_1}{3p^{\frac{2}{3}}T^{a_2}} - \frac{2a_3}{3p^{\frac{1}{3}}T} + \frac{a_4}{T} - \frac{a_5 a_6 p^{a_6}}{pT} \tag{11}$$

As illustrated in Fig. 14, the impact of temperature on the isothermal compressibility coefficient is rather subtle. This suggests that variations in temperature within the examined range do not induce significant shifts in the coefficient's value. Furthermore, all the isotherms converge and can be represented by a single unified line for pressures up to approximately 20 MPa. This convergence highlights H_2's consistent compressibility across those temperatures, underscoring temperature's minimal impact within the observed pressure range. Fig. S1 provides a detailed analysis of the AD% associated with Eq. (10) for predicting the isothermal compressibility coefficient, drawing comparisons with data sourced from REFPROP 10 (Lemmon et al., 2018).

Table 10. Statistical metrics for various methods used in estimating H_2 thermal conductivity.

Properties	AAD%	MaxAD%	R^2	PAP
Density (ρ)	0.263	3.292	0.99917	99.80
Viscosity (μ)	1.158	11.51	0.99828	99.12
Thermal conductivity (λ)	1.353	10.66	0.99818	98.99
Isothermal compressibility coefficient (κ_T)	0.632	7.874	1	99.55
Coefficient of volume expansion (α_p)	0.967	8.590	0.9979	99.26
Fugacity coefficient (φ)	1.394	4.405	0.99777	98.92
Enthalpy (H)	0.646	4.541	0.99997	99.54
Entropy (S)	0.802	5.724	0.99923	99.42
Helmholtz energy (A)	0.792	7.201	0.9997	99.44
Gibbs energy (G)	1.119	8.806	0.99965	98.55
Isobaric heat capacity (C_p)	0.912	4.328	0.71663	46.31
Heat capacity ratio (γ)	0.81	6.030	0.90679	84.55
Adiabatic bulk modulus (B_S)	1.26	9.150	0.99779	99.09
Speed of sound (w)	0.603	4.089	0.99867	99.54
Kinematics viscosity (ν)	1.216	10.48	0.99998	99.14
Thermal diffusivity (h)	2.035	15.16	0.99999	98.56

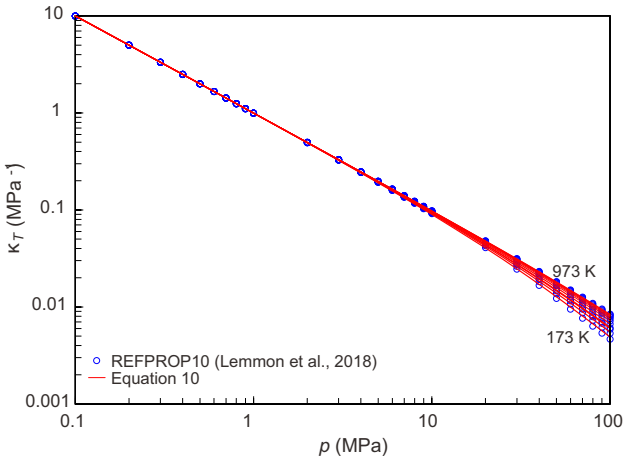

Fig. 14. Comparison of performance of Eq. (10) with data from REFPROP 10 (Lemmon et al., 2018) for estimating the isothermal compressibility coefficient.

From this visual representation, it becomes evident that the predictive accuracy of Eq. (10) is notably high for temperatures above 225 K. Regardless of pressure variations, the isothermal compressibility coefficient predictions consistently yield an absolute error of less than 2%. Although the accuracy remains acceptable, the prediction errors reach up to 7.8% at temperatures less than 225 K and pressures higher than 30 MPa.

4.2 Gas volume expansivity

The gas volume expansivity (α_p) plays a pivotal role across numerous scientific, engineering, and industrial fields. Accurate predictions of the variations in gas volume with temperature is important in system design, and performance optimization (Yang et al., 2023). Often referred to as the coefficient of volume expansion or the thermal expansion coefficient, the gas volume expansivity quantifies the rate at which a gas's volume changes in response to shifts in temperature (Al-Yaseri et al., 2021). The coefficient of volume expansion is defined as:

$$\alpha_p = \frac{1}{T} + \frac{\left(\frac{\partial Z}{\partial T}\right)_p}{Z} \tag{12}$$

where

$$\left(\frac{\partial Z}{\partial T}\right)_p = \frac{a_1 a_2 p^{\frac{1}{3}}}{T^{1+a_2}} + \frac{a_3 p^{\frac{2}{3}}}{T^2} + \frac{a_4 p}{T^2} + \frac{a_5 p^{a_6}}{T^2} \tag{13}$$

As depicted in Figs. 15 and S2, the coefficient can be accurately represented up to the freezing point of water using Eq. (12), yielding an absolute deviation below 3% across the examined pressure spectrum. Nonetheless, accuracy diminishes for temperatures below this threshold. Specifically, the discrepancy amplifies at pressures surpassing 70 MPa with temperatures under 173 K and pressures ranging from 10 to 30 MPa at temperatures below 200 K. However, absolute deviations remain below 8.5%.

4.3 Fugacity coefficient

The fugacity coefficient (φ), which closely relates to variations in chemical potentials and molar Gibbs energies, is delineated by the Gibbs-Duhem equation (Tosun, 2021). Based on Eq. (4), this coefficient can be expressed as:

$$\varphi = \exp\left(\frac{a_4 p}{T} - \frac{3a_1 p^{\frac{1}{3}}}{T^{a_2}} - \frac{3a_3 p^{\frac{2}{3}}}{2T} - \frac{a_5 p^{a_6}}{a_6 T}\right) \tag{14}$$

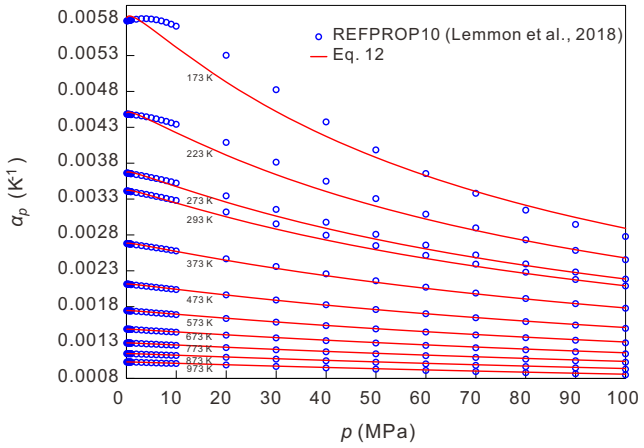

Fig. 15. Performance of Eq. (12) versus data generated using REFPROP10 (Lemmon et al., 2018) in estimating the gas volume expansivity coefficient.

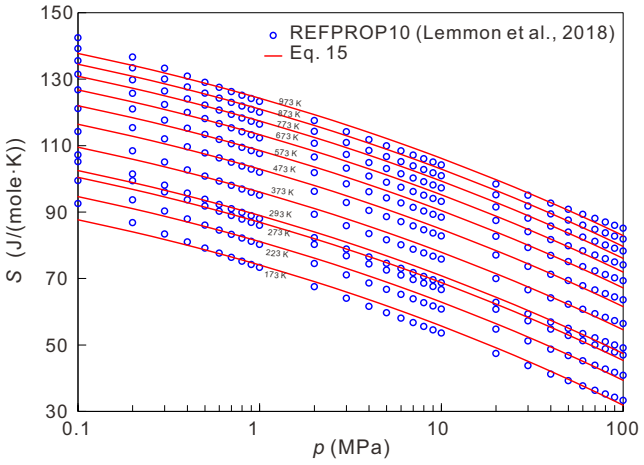

Fig. 16. Performance of Eq. (15) for estimating the entropy of H_2 generated by REFPROP 10 (Lemmon et al., 2018).

Fig. S3 depicts Eq. (14)'s predictions of the fugacity coefficient against data from REFPROP 10 (Lemmon et al., 2018). While deviations are evident for temperatures below 200 K and pressures under 10 MPa, they remain below 4.5%. For temperatures between 200 and 400 K, the absolute deviation remains under 2.5%; for higher temperatures, it's less than 1.5%.

4.4 Entropy and enthalpy

The variations in entropy (S) and enthalpy (H) of H_2 during processes such as compression (Sun et al., 2023) and adsorption (Mizutani et al., 2023) are pivotal for in-depth thermodynamic assessments. This understanding is vital for elucidating system dynamics, enhancing operational performance, and safeguarding during H_2 handling and application. As derived from Eq. (4), these properties can be represented as:

$$S = S^0 + R\left(-3a_1 p^{\frac{1}{3}}(a_2 - 1)T^{-a_2}\right) \tag{15}$$

and

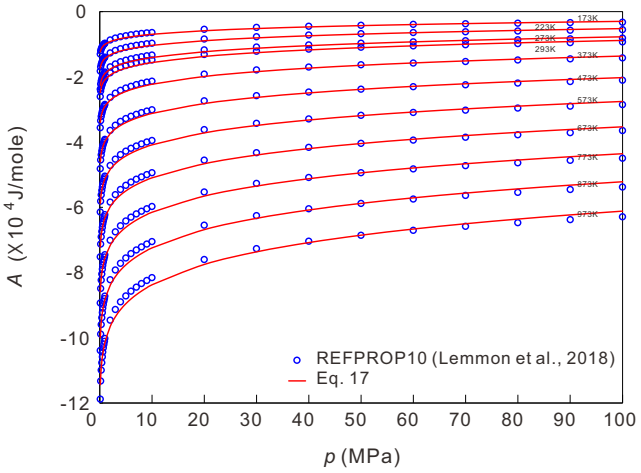

Fig. 17. Evaluation of Eq. (17) in predicting the Helmholtz energy of H_2, based on data generated by REFPROP 10 (Lemmon et al., 2018).

$$H = H^0 + R\left(-\frac{a_3 p^{\frac{2}{3}}}{2T} - \frac{3a_1 a_2 p^{\frac{1}{3}}}{T^{a_2}} - \frac{a_5 p^{a_6}}{a_6 T} + \frac{a_4 p}{T}\right) \tag{16}$$

Fig. 16 illustrates the efficacy of Eq. (15) in estimating the entropy of H_2. While the estimation deviation for this equation does not exceed 5%, as detailed in Table 10, it is evident that the calculated values are consistently underestimated for pressures below 1 MPa.

Fig. S4 presents the AD% of Eq. (16) for estimating H_2 enthalpy, benchmarked against data from REFPROP 10 (Lemmon et al., 2018). For temperatures exceeding 273 K, this equation predicts enthalpy values with a deviation of less than 1.5%, irrespective of pressure. Although deviations emerge for temperatures below 273 K and pressures surpassing 15 MPa, they consistently remain below 4.5%.

4.5 Helmholtz energy

The Helmholtz energy (A) of H_2 is fundamental for understanding its thermodynamic behavior, such as its rapid depressurization or compression. A can be calculated as:

$$A = A^0 + R\left(-\frac{a_3 p^{\frac{2}{3}}}{2} - \frac{a_5 p^{a_6}}{a_6} - \frac{2a_1 p^{\frac{1}{3}}}{T^{a_2-1}} + a_5 p^{a_6} - T\right) \tag{17}$$

where A^0 represents the Helmholtz energy of an ideal gas. Using Eqs. (7) and (8), A^0 can be expressed as (for constants, see Table 6):

$$A^0 = -e_1 - d_1 T(\ln(T) - 1) + T\left(d_2 \ln\left(\sinh\left(\frac{d_3}{T}\right)\right) - d_4 \ln\left(\cosh\left(\frac{d_5}{T}\right)\right) + e_2 \ln^{e_3}(p)\right) \tag{18}$$

Fig. 17 illustrates the effectiveness of Eq. (17) in estimating the Helmholtz energy of H_2 based on data generated by REFPROP 10 (Lemmon et al., 2018).

The relationship between Helmholtz and Gibbs energies is fundamental for many applications, spanning from hydrogen production to subsurface storage operations. Given Eqs. (17) and (4), the Gibbs energy of H_2 can be succinctly repre-

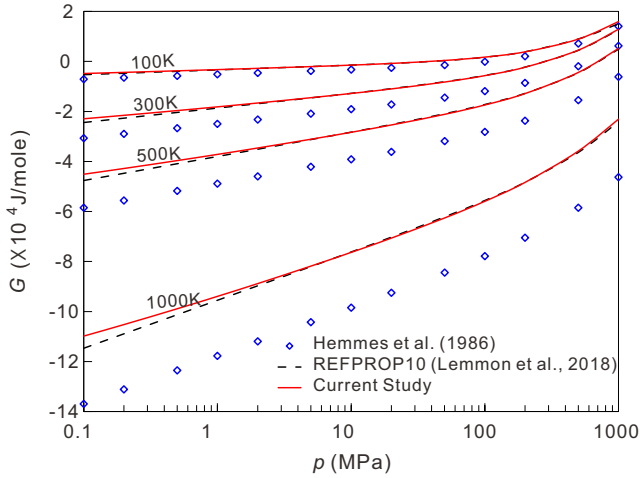

Fig. 18. Comparison of the proposed correlation for estimating the Gibbs energy of H_2 with values generated by REFPROP 10 (Lemmon et al., 2018) and results presented by Hemmes et al. (1986).

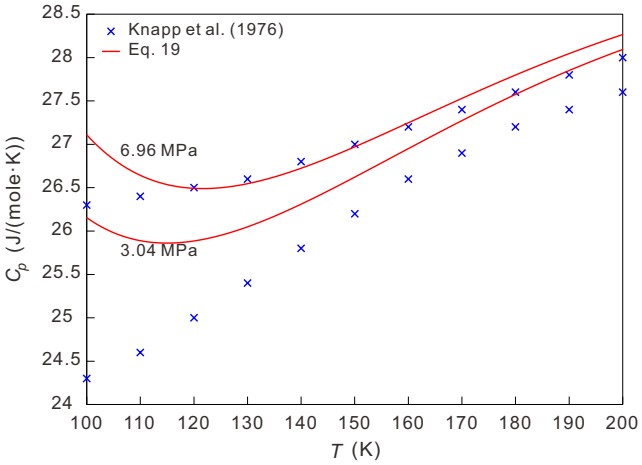

Fig. 19. Comparison of the current study's results with data from Knapp et al. (1976) for estimating the isobaric heat capacity of H_2.

sented as $G = A + ZRT$. The calculated values for the Gibbs energy of H_2 across four isotherms are compared in Fig. 18 with data from REFPROP 10 (Lemmon et al., 2018) and findings by Hemmes et al. (1986). The results of this study agree with those from REFPROP 10 (Lemmon et al., 2018). Results from Hemmes et al. (1986), used as benchmark data by Joubert (2010), show lower values and this discrepancy is amplified at elevated temperatures.

4.6 Isobaric heat capacity

Second derivative properties are significant in scientific and engineering domains, yet their accurate determination remains challenging (Shoghl et al., 2020). The complexity intensifies when simple empirical correlations come into play. Nonetheless, their importance is such that engineering computations cannot overlook them (Li et al., 2023a). Using Eqs. (4) and (7), the isobaric heat capacity (C_p) of H_2 can be calculated as:

$$C_p = C_p^0 + R\left(3a_1a_2p^{\frac{1}{3}}(a_2-1)T^{-a_2}\right) \tag{19}$$

Fig. 19 shows the results of Eq. (19) compared with experimental data from Knapp et al. (1976) for two different isobars of 3.04 and 6.96 MPa. Given that C_p is a second-order derivative property and the simplicity of Eq. (4), the results shown in Fig. 19 are acceptable.

The heat capacity ratio (γ), which is intrinsically connected to variations in internal energy and often derived from the relationship between the isobaric and isochoric heat capacities, can also be expressed as:

$$\gamma = \frac{C_p^0 + R\left(3a_1a_2p^{\frac{1}{3}}(a_2-1)T^{-a_2}\right)}{C_p^0 + R\left(3a_1a_2p^{\frac{1}{3}}(a_2-1)T^{-a_2} + \frac{3p^{\frac{2}{3}}\left(a_1(a_2-1)p^{\frac{1}{3}}+T^{a_2}\right)^2T^{1-a_2}}{2a_1Tp+a_3p^{\frac{4}{3}}T^{a_2}-3T^{1+a_2}p^{\frac{2}{3}}-3a_5T^{a_2}(a_6-1)p^{a_6+\frac{2}{3}}}\right)} \tag{20}$$

From a geophysical perspective, acoustic waves propagate swiftly through fluids, suggestive of an adiabatic process (Batzle and Wang, 1992). Consequently, accurate estimates of the adiabatic bulk modulus ($B_s = \gamma/\kappa_T$) is important when using geophysical models to explore and characterize subsurface reservoirs and storage sites.

Fig. 20 illustrates the variation in the adiabatic bulk modulus of H_2. Analogous to the isothermal compressibility, it can be represented by a single line for pressures up to 20 MPa. However, as pressure increases, the bulk modulus also rises, whereas an increase in temperature leads to a decrease in the modulus. Estimating the adiabatic bulk modulus of H_2 using the current study yields an error of less than four percent for temperatures above 300 K across all pressure values. However, the error escalates to approximately 9% at temperatures lower than 300 K.

In addition to density and bulk modulus, the speed of sound ($w^2 = B_s/\rho_m$; ρ_m is the mass-based density of H_2) is an essential thermodynamic property used in seismic characterization (Carvalho and Moraes, 2021). Fig. 21 shows that increasing either pressure or temperature (except at high pressure and low temperature values) leads to an increase in the speed of sound in H_2, as observed in the results from REFPROP 10 (Lemmon et al., 2018).

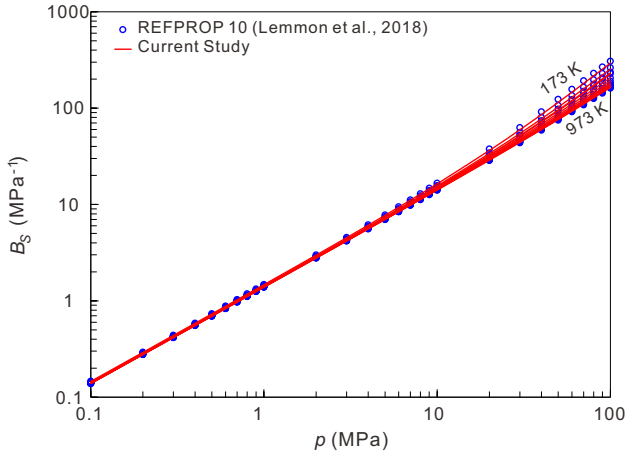

Fig. 20. Comparison of the current study's results with data generated by REFPROP 10 (Lemmon et al., 2018) for estimating the adiabatic bulk modulus of H_2.

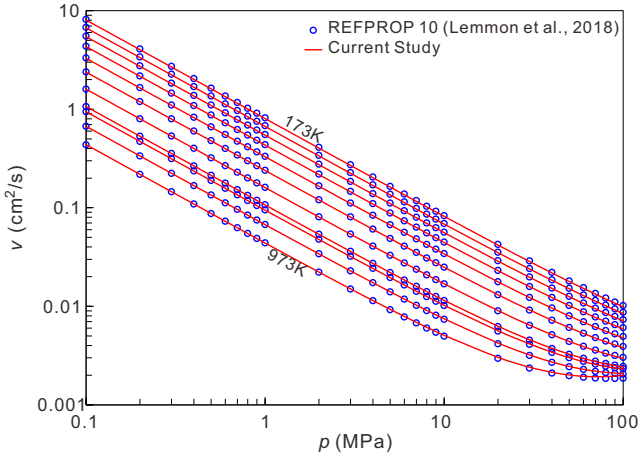

Fig. 22. Performance of currently developed equations versus data generated using REFPROP 10 (Lemmon et al., 2018) in estimating the kinematic viscosity.

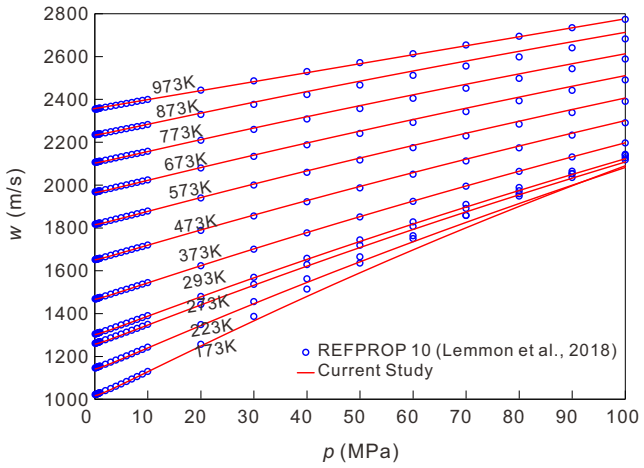

Fig. 21. Comparison of the current equations with data from REFPROP 10 (Lemmon et al., 2018) in estimating the speed of sound in H_2.

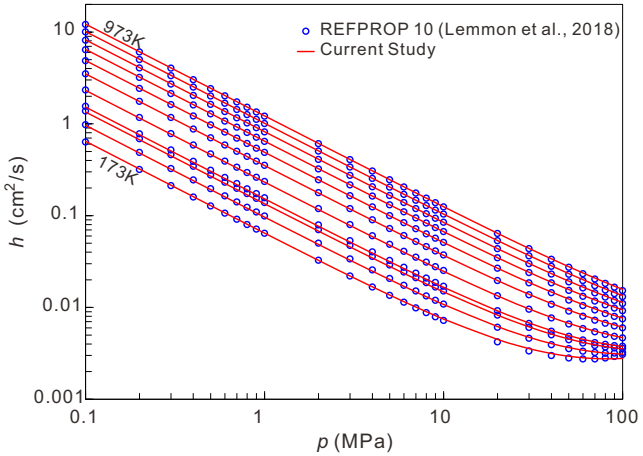

Fig. 23. Performance of currently developed equations versus data generated using REFPROP 10 (Lemmon et al., 2018) in estimating thermal diffusivity.

4.7 Kinematic viscosity and thermal diffusivity

As a measure of a fluid's internal resistance to flow under gravitational forces, the kinematic viscosity ($\nu = \mu/\rho$) of H_2 is crucial in determining its flow behavior, heat transfer capabilities, energy efficiency, and mixing characteristics (Bang et al., 2023). Fig. 22 demonstrates the performance of the developed correlations in predicting the kinematic viscosity data generated by REFPROP 10 (Lemmon et al., 2018).

The Prandtl number for H_2, as per REFPROP 10 (Lemmon et al., 2018), lies between 0.62 and 0.69 for the temperature and pressure ranges explored in this study. Such values underscore the significance of thermal diffusivity (Wang et al. 2023). Thermal diffusivity, represented as ($h = \lambda/(\rho \cdot C_p)$), quantifies a material's propensity to conduct thermal energy in relation to its thermal storage capacity. It is computed by dividing the thermal conductivity by the product of density and the specific heat capacity at constant pressure. Fig. 23 shows that REFPROP 10 (Lemmon et al., 2018) reproduces the thermal diffusivity data well.

Table 10 summarizes the statistical parameters for the models developed in this study compared to results generated by REFPROP 10 (Lemmon et al., 2018). As mentioned earlier, 8,600 data points were generated for each property. Among the derived properties, the speed of sound and the isothermal compressibility coefficient exhibit the lowest average deviations. Conversely, compared to results generated by REFPROP 10 (Lemmon et al., 2018), the proposed correlation performs least favorably in estimating the derived properties, thermal diffusivity, and fugacity coefficient. Additionally, based on the PAP values, estimates of the isobaric heat capacity and the heat capacity ratio are not as reliable. While the predictions of the proposed model are generally close to the reference values, the model does not capture the underlying variability in the data well. It is worth highlighting that the data used in REFPROP 10 (Lemmon et al., 2018), as represented in the Figures and Table 10, are calculated using a multiparameter EoS.

Based on the error analysis, the proposed models provide accurate estimations and perform well across a wide range of

conditions.

5. Conclusions

To understand the thermodynamic and transport properties of gaseous hydrogen, this work has developed easy-to-use, mathematical relations to estimate various properties of H_2. These properties include the compressibility factor, viscosity, thermal conductivity, and ideal gas isobaric heat capacity/enthalpy/entropy. The calculated compressibility factor shows how hydrogen deviates from an ideal gas, with the deviation typically falling within one percent. More significant deviations are observed at lower temperatures and pressures. The viscosity and thermal conductivity of hydrogen are modeled using a power law as functions of temperature and pressure, with deviations generally below two percent. These correlations, benchmarked against experimental data and the REFPROP 10 database, provide efficient and accurate estimations for a broad spectrum of thermodynamic properties of hydrogen.

For each correlation, statistical metrics such as AAD%, MaxAD%, R^2, and PAP have been calculated. The results demonstrate the efficacy, reliability, and applicability of the developed models and their agreement with experimental data and derived properties. It is also important to acknowledge the inherent limitations of the models. For instance, while the isobaric heat capacity and heat capacity ratio predictions are generally accurate, they do exhibit deviations under specific conditions.

The models consistently perform well across a wide range of conditions, capturing the intrinsic behavior of properties such as the isothermal compressibility coefficient and the speed of sound in hydrogen. This study illuminates the relationships between hydrogen's thermodynamic properties and explores its derived properties. In the broader context, this work contributes to the expanding knowledge base on hydrogen. Due to their accuracy and reliability, the proposed models will serve as valuable tools to design efficient hydrogen storage systems, optimize hydrogen-centric energy solutions, and further our understanding of hydrogen's thermodynamic properties.

Acknowledgements

This work was supported by the School of Energy Resources Hydrogen Research Center (SER H2ERC) at the University of Wyoming. The corresponding author thanks Director Eugene Holubnyak for our lively discussions.

Supplementary file

https://doi.org/10.46690/ager.2024.01.05

Conflict of interest

The authors declare no competing interest.

References

Aly, F. A., Lee, L. L. Self-consistent equations for calculating the ideal gas heat capacity, enthalpy, and entropy. Fluid Phase Equilibria, 1981, 6(3-4): 169-179.

Al-Yaseri, A., Wolff-Boenisch, D., Fauziah, C. A., et al. Hydrogen wettability of clays: Implications for underground hydrogen storage. International Journal of Hydrogen Energy, 2021, 46(69): 34356-34361.

Amagat, E. H. Mémoires sur l'élasticité et la dilatation des fluides jusqu'aux très hautes pressions. Annales de Chimie et de Physique, 1893, 29: 505-574.

Aryana, S. A., Kovscek, A. R. Experiments and analysis of drainage displacement processes relevant to carbon dioxide injection. Physical Review E, 2012, 86(6): 066310.

Assael, M. J., Assael, J. -A. M., Huber, M. L., et al. Correlation of the thermal conductivity of normal and parahydrogen from the triple point to 1000 K and up to 100 MPa. Journal of Physical and Chemical Reference Data, 2011, 40(3): 033101.

Assael, M. J., Mixafendi, S., Wakeham, W. A. The viscosity and thermal conductivity of normal hydrogen in the limit of zero density. Journal of Physical and Chemical Reference Data, 1986, 15(4): 1315-1322.

Assael, M. J., Wakeham, W. A. Thermal conductivity of four polyatomic gases. Journal of the Chemical Society, Faraday Transactions 1: Physical Chemistry in Condensed Phases, 1981, 77(3): 697-707.

Bartlett, E. P. The compressibility isotherms of hydrogen, nitrogen and mixtures of these gases at 0 and pressures to 1000 atmospheres. Journal of the American Chemical Society, 1927, 49(3): 687-701.

Bartlett, E. P., Cupples, H. L., Tremearne, T. H. The compressibility isotherms of hydrogen, nitrogen and a 3:1 mixture of these gases at temperatures between 0 and 400 and at pressures to 1000 atmospheres. Journal of the American Chemical Society, 1928, 50(5): 1275-1288.

Bartlett, E. P., Hetherington, H. C., Kvalnes, H. M., et al. The compressibility isotherms of hydrogen, nitrogen and a 3:1 mixture of these gases at temperatures of -70, -50, -25 and 20 and at pressures to 1000 atmospheres. Journal of the American Chemical Society, 1930, 52(4): 1363-1373.

Bartolomeu, R. A., Franco, L. F. Thermophysical properties of supercritical H_2 from Molecular Dynamics simulations. International Journal of Hydrogen Energy, 2020, 45(33): 16372-16380.

Barua, A. K., Afzal, M., Flynn, G. P., et al. Viscosity of hydrogen, deuterium, methane, and carbon monoxide from -50° to 150 °C below 200 atmospheres. The Journal of Chemical Physics, 1964, 41(2): 374-378.

Batzle, M., Wang, Z. Seismic properties of pore fluids. Geophysics, 1992, 57(11): 1396-1408.

Boyd Jr, J. H. The viscosity of compressed gases. Physical Review, 1930, 35(10): 1284-1297.

Bridgman, P. W. The Compressibility of Five Gases to High Pressures. Cambridge, USA, Harvard University Press, 1924.

Carey, C., Carnevale, E. H., Uva, S., et al. Experimental

Determination of Gas Properties at High Temperatures and/or Pressures. Alexandria, USA, National Technical Information Service, 1974.

Chase, M. W., Davies, C. A., Downey, J. R., et al. JANAF thermochemical tables, Third Edition. Journal of Physical and Chemical Reference Data, 1985, 14: 927-1856.

Chen, H., Zheng, J., Xu, P., et al. Study on real-gas equations of high pressure hydrogen. International Journal of Hydrogen Energy, 2010, 35(7): 3100-3104.

Chen, M., Al-Subhi, K., Al-Rajhi, A., et al. Numerical evaluation of hydrogen production by steam reforming of natural gas. Advances in Geo-Energy Research, 2023, 7(3): 141-151.

Cheng, S., Li, F., Shang, F., et al. A review of experimental researches on the thermophysical properties of hydrogen-containing mixtures at high temperatures and high pressures. Journal of Chemical & Engineering Data, 2021, 66(9): 3361-3385.

Cheng, S., Shang, F., Ma, W., et al. PVT Measurements of the H_2-CO_2-CH_4-CO-H_2O system at 740-939 K and 18.1-34.7 MPa with an isochoric apparatus and the development of a virial equation of state. Journal of Chemical & Engineering Data, 2020, 65(10): 4881-4891.

Chu, H., Ma, T., Zhu, W., et al. A novel semi-analytical monitoring model for multi-horizontal well system in large-scale underground natural gas storage: Methodology and case study. Fuel, 2023, 334, 126807.

Chuang, S. Y., Chappelear, P. S., Kobayashi, R. Viscosity of methane, hydrogen, and four mixtures of methane and hydrogen from -100.degree.C to 0.degree.C at high pressures. Journal of Chemical & Engineering Data, 1976, 21(4): 403-411.

Clerc, H., Tufeu, R., Neindre, B. Le, Proceedings of the 7th Symposium on Thermophysical Properties, Gaithersburg, MD, USA, 1977.

Clifford, A. A., Colling, L., Dickinson, E., et al. Testing intermolecular potential functions using transport property data. Part 2.-Thermal conductivities of mixtures of helium with the hydrogen isotopes. Journal of the Chemical Society, Faraday Transactions 1: Physical Chemistry in Condensed Phases, 1975, 71: 1962-1977.

Clifford, A. A., Kestin, J., Wakeham, W. A. The viscosity of mixtures of hydrogen with three noble gases. Berichte Der Bunsengesellschaft Für Physikalische Chemie, 1981, 85(5): 385-388.

Clifford, A. A., Platts, N. Calculation of the thermal conductivities of hydrogen, nitrogen, oxygen and carbon dioxide at high temperatures. Journal of the Chemical Society, Faraday Transactions 1: Physical Chemistry in Condensed Phases, 1981, 77(11): 2669-2678.

Davarnejad, R., Rahimi, B., Baghban, S. N., et al. Development of a thermodynamic model for hydrogen and hydrogen containing mixtures. Fluid Phase Equilibria, 2014, 382: 1-9.

De Lucia, M., Pilz, P., Liebscher, A., et al. Measurements of H_2 solubility in saline solutions under reservoir conditions: Preliminary results from project H2STORE. Energy Procedia, 2015, 76: 487-494.

Diller, D. E. Measurements of the viscosity of parahydrogen. The Journal of Chemical Physics, 1965, 42(6): 2089-2100.

Elliott, J. R., Vladimir, D., Knotts, I. V., et al. Properties of Gases and Liquids. New York, USA, McGraw Hill, 2023.

Golubev, I. F.; Shepeleva, R. I. Viscosity of hydrogen at low temperatures and high pressures. Gazovaya Promyshlennost 1966, 11(4), 54-58. (in Russian)

Golubev, I. F., Shepeleva, R. I. Gazovaya Promyshlennost, 1966, 11(4): 54-58.

Goria, K., Singh, H. M., Singh, A., et al. Insights into biohydrogen production from algal biomass: Challenges, recent advancements and future directions. International Journal of Hydrogen Energy, 2024, 52: 127-151.

Gracki, J. A., Flynn, G. P., Ross, J. Viscosity of nitrogen, helium, hydrogen, and argon from -100 to 25°C up to 150-250 atm. The Journal of Chemical Physics, 1969, 51(9): 3856-3863.

Green hydrogen: An alternative that reduces emissions and cares for our planet, 2023.

Guo, F., Aryana, S. A. An experimental investigation of flow regimes in imbibition and drainage using a microfluidic platform. Energies, 2019, 12(7): 1390.

Haas, W. D., Onnes, H. K. Isotherms of diatomic substances and of their binary mixtures. XII. The compressibility of hydrogen vapour at, and below the boiling point. KNAW, Proceedings, 1912, 15: 405-417.

Han, Y., Fan, C., Yin, Y., et al. Cooperative hydrogen- and halogen-bonding interaction promoted deep eutectic solvent-functionalized magnetic metal-organic framework for perfluoroalkyl iodides detection in edible oils. Food Control, 2023, 148: 109625.

Hanley, H. J. M., McCarty, R. D., Intemann, H. The viscosity and thermal conductivity of dilute gaseous hydrogen from 15 to 5000 K. Journal of Research of the National Bureau of Standards. Section A, Physics and Chemistry, 1970, 74(3): 331-353.

Heidaryan, E. A note on model selection based on the percentage of accuracy-precision. Journal of Energy Resources Technology, 2019, 141(4): 045501.

Hematpur, H., Abdollahi, R., Rostami, S., et al. Review of underground hydrogen storage: Concepts and challenges. Advances in Geo-Energy Research, 2023, 7(2): 111-131.

Hemmes, H., Driessen, A., Griessen, R. Thermodynamic properties of hydrogen at pressures up to 1 Mbar and temperatures between 100 and 1000K. Journal of Physics C: Solid State Physics, 1986, 19(19): 3571.

Hemminger, W. The thermal conductivity of gases: Incorrect results due to desorbed air. International Journal of Thermophysics, 1987, 8: 317-333.

Holborn, L., Otto, J. Über die Isothermen einiger Gase zwischen +400° und -183°. Zeitschrift für Physik, 1925, 33: 1-11. (in Chinese)

Huppmann, D., Smith, C. Mitigation pathways compatible with 1.5 °C in the context of sustainable development, in Global Warming of 1.5 °C, Intergovernmental Panel on Climate Change, edited by J. Rogelj, D. Shindell, K. Jiang, et al., Cambridge University Press, Cambridge, pp.

93-174, 2018.

Intergovernmental Panel on Climate Change (IPCC). Mitigation pathways compatible with 1.5 °C in the context of sustainable development, in Global Warming of 1.5 °C, 2018, pp. 93-174.

IRENA, Hydrogen, 2023.

Jaeschke, M., Humphreys, A. E. The GERG Databank of High Accuracy Compressibility Factor Measurements. Düsseldorf, Germany, VDI Verl., 1991.

Jarrahian, A., Karami, H. R., Heidaryan, E. On the isobaric specific heat capacity of natural gas. Fluid Phase Equilibria, 2014, 384: 16-24.

Johnston, H. L., McCloskey, K. E. Viscosities of several common gases between 90 °K and room temperature. The Journal of Physical Chemistry, 1940, 44(9): 1038-1058.

Johnston, H. L., White, D., Wirth, H., et al. Cryogenic Laboratory, Ohio State University Report No. 264-25, 1953.

Jossi, J. A., Stiel, L. I., Thodos, G. The viscosity of pure substances in the dense gaseous and liquid phases. AIChE Journal, 1962, 8(1): 59-63.

Joubert, J. M. A Calphad-type equation of state for hydrogen gas and its application to the assessment of Rh-H system. International Journal of Hydrogen Energy, 2010, 35(5): 2104-2111.

Katalenich, S. M., Jacobson, M. Z. Toward battery electric and hydrogen fuel cell military vehicles for land, air, and sea. Energy, 2022, 254: 124355.

Kestin, J., Nagashima, A. The viscosity of the isotopes of hydrogen and their intermolecular force potentials. Physics of Fluids, 1964, 7 (5): 730-734.

Kestin, J., Ro, S. T., Wakeham, W. A. Reference values of the viscosity of twelve gases at 25 °C. Transactions of the Faraday Society, 1971, 67: 2308-2313.

Kestin, J., Wang, H. The viscosity of five gases: A re-evaluation. Transactions of the American Society of Mechanical Engineers, 1958, 80(1): 11-17.

Kestin, J., Yata, J. Viscosity and diffusion coefficient of six binary mixtures. The Journal of Chemical Physics, 1968, 49(11): 4780-4791.

Knapp, H., Schmölling, K., Neumann, A. Measurement of the molal heat capacity of H_2-N_2 mixtures. Cryogenics, 1976, 16(4): 231-237.

Kuss, E. High pressure research II: The viscosity of compressed gases. Zeitschrift Fur Angewandte Mathematik Und Physik, 1952, 4(6): 203-207.

Leachman, J. W., Jacobsen, R. T., Penoncello, S. G., et al. Fundamental equations of state for parahydrogen, normal hydrogen, and orthohydrogen. Journal of Physical and Chemical Reference Data, 2009, 38(3): 721-748.

Lemmon, E. W., Bell, I. H., Huber, M. L., et al. NIST standard reference database 23: Reference fluid thermodynamic and transport properties-REFPROP, Version 10.0, 2018.

Lemmon, E. W., Huber, M. L., Friend, D. G., et al. Standardized Equation for Hydrogen Gas Densities for Fuel Consumption Applications 1. SAE International, USA, 2006.

Lemmon, E. W., Huber, M. L., Leachman, J. W. Revised standardized equation for hydrogen gas densities for fuel consumption applications. Journal of Research of the National Institute of Standards and Technology, 2008, 113(6): 341-350.

Leneindr. B. Experimental study of thermal-conductivity of some fluids at high-temperature and pressure. International Journal of Heat and Mass Transfer, 1972, 15(1): 1-24.

Li, J., Chen, Y., Ma, Y., et al. A study on the Joule-Thomson effect of during filling hydrogen in high pressure tank. Case Studies in Thermal Engineering, 2023a, 41: 102678.

Li, F., Ma, W., Zhang, X. Database of thermophysical properties of H_2/CO_2/CO/CH_4/H_2O mixtures. International Journal of Hydrogen Energy, 2023b, 48(44): 16923-16935.

Liebenberg, D. H., Mills, R. L., Bronson, J. C. Thermodynamic properties of fluid nH_2 in the range 75 to 307 K and 2 to 20 kbar. Los Alamos National Lab (LANL), Los Alamos, NM, United States, 1977.

Liebenberg, D. H., Mills, R. L., Bronson, J. C. Measurement of P,V,T, and sound velocity across the melting curve of n-H_2 and n-D_2 to 19 kbar. Physical Review B, 1978, 18(8): 4526-4532.

Liu, L., Nieto-Draghi, C., Lachet, V., et al. Bridging confined phase behavior of CH_4-CO_2 binary systems across scales. The Journal of Supercritical Fluids, 2022, 189: 105713.

Liu, Y., Li, Y., Ma, H., et al. Detection and evaluation technologies for using existing salt caverns to build energy storage. Energies, 2022a, 15(23): 9144.

Lukin, V. I., Ivakin, B. A., Suetin, P. E. Temperature dependence of the viscosity coefficients of some gases. Soviet Physics-Technical Physics, 1983, 28(5): 597. (in Russian)

Mal'tsev, V. A., Nerushev, O. A., Novopashin, S. A., et al. Viscosity of H_2-CO_2 mixtures at (500, 800, and 1100) K. Journal of Chemical & Engineering Data, 2004, 49(3): 684-687.

May, E. F., Berg, R. F., Moldover, M. R. Reference viscosities of H_2, CH_4, Ar, and Xe at low densities. International Journal of Thermophysics, 2007, 28(4): 1085-1110.

McCarty, R. D. Thermophysical Properties of Parahydrogen from the Freezing Liquid Line to 5000 R for Pressures to 10,000 psia. Washington, D. C., USA, US Department of Commerce, 1972.

Mehl, J. B., Huber, M. L., Harvey, A. H. Ab initio transport coefficients of gaseous hydrogen. International Journal of Thermophysics, 2010, 31(4-5): 740-755.

Menabde, N. E. Viscosity coefficient of hydrogen (H_2, D_2), neon (Ne^{20}, Ne^{22}) and helium (He^3) isotopes in the temperature range -195 to +25 °C. Soviet Atomic Energy, 1965, 19(5): 1421-1422.

Michels, A., De Graaff, W., Wassenaar, T., et al. Compressibility isotherms of hydrogen and deuterium at temperatures between -175 °C and +150 °C (at densities up to 960 amagat). Physica, 1959, 25(1-6): 25-42.

Michels, A., Goudeket, M. Compressibilities of deuterium between 0 °C and 150 °C, up to 3000 atmospheres. Physica, 1941, 8(3): 353-360.

Michels, A., Schipper, A. C. J., Rintoul, W. H. The viscosity of hydrogen and deuterium at pressures up to 2000 atmospheres. Physica, 1953, 19: 1011-1028.

Millat, J., Dymond, J. H., de Castro, C. N., et al. Transport Properties of Fluids. Cambridge, United Kingdom, Cambridge University Press, 1996.

Mills, R. L., Liebenberg, D. H., Bronson, J. C., et al. Equation of state of fluid n-H_2 from P-V-T and sound velocity measurements to 20 kbar. The Journal of Chemical Physics, 1977, 66(7): 3076-3084.

Mizutani, T., Ohta, H., Ueda, T., et al. Mechanochemically tailored silicon particles for efficient H_2 production: Entropy and enthalpy engineering. ACS Sustainable Chemistry & Engineering, 2023, 11(32): 11769-11780.

Moroe, S., Woodfield, P. L., Kimura, K., et al. Measurements of hydrogen thermal conductivity at high pressure and high temperature. International Journal of Thermophysics, 2011, 32: 1887-1917.

Mustafa, M., Ross, M., Trengove, R. D., et al. Absolute measurement of the thermal conductivity of helium and hydrogen. Physica A: Statistical Mechanics and its Applications, 1987, 141(1): 233-248.

Muzny, C. D., Huber, M. L., Kazakov, A. F. Correlation for the viscosity of normal hydrogen obtained from symbolic regression. Journal of Chemical & Engineering Data, 2013, 58(4): 969-979.

Nabizadeh, H., Mayinger, F. Viscosity of binary mixtures of hydrogen and natural gas (hythane) in the gaseous phase. High Temperatures-High Pressures, 1999, 31(6): 601-612.

Negro, V., Noussan, M., Chiaramonti, D. The potential role of ammonia for hydrogen storage and transport: A critical review of challenges and opportunities. Energies, 2023, 16(17): 6192.

Nguyen, T. B., Sherpa, K., Chen, C. W., et al. Breakthroughs and prospects in ruthenium-based electrocatalyst for hydrogen evolution reaction. Journal of Alloys and Compounds, 2023, 968: 172020.

Park, B. H., Chae, C. K. Development of correlation equations on hydrogen properties for hydrogen refueling process by machine learning approach. International Journal of Hydrogen Energy, 2022, 47(6): 4185-4195.

Presnall, D. C. Pressure-volume-temperature measurements on hydrogen from 200 to 600 °C and up to 1800 atmospheres. Journal of Geophysical Research, 1969, 74(25): 6026-6033.

Qiu, Z., Yue, Q., Yan, T., et al. Gas utilization optimization and exergy analysis of hydrogen metallurgical shaft furnace. Energy, 2023, 263: 125847.

Reed, T. M., Gubbins, K. E. Applied Statistical Mechanics: Thermodynamic and Transport Properties of Fluids. New York, USA, McGraw Hill, 1973.

Roder, H. M. Thermal conductivity of hydrogen for temperatures between 78 and 310 K with pressures to 70 MPa. International Journal of Thermophysics, 1984, 5: 323-350.

Roder, H. M., Diller, D. E. Thermal conductivity of gaseous and liquid hydrogen. The Journal of Chemical Physics, 1970, 52(11): 5928-5949.

Rudenko, N. S., Sliusar, V. Viscosity of hydrogen at constant density over the temperature range 16.6-300 deg K. Ukrainian Physics Journal, 1968, 13: 656-659.

Sakoda, N., Hisatsugu, T., Furusato, K., et al. Viscosity measurements of hydrogen at high temperatures up to 573 K by a curved vibrating wire method. The Journal of Chemical Thermodynamics, 2015, 89: 22-26.

Sakoda, N., Shindo, K., Motomura, K., et al. Burnett PVT measurements of hydrogen and the development of a virial equation of state at pressures up to 100 MPa. International Journal of Thermophysics, 2012, 33: 381-395.

Scott, G. A. The isotherms of hydrogen, carbon monoxide and their mixtures. Proceedings of the Royal Society of London, Series A, Containing Papers of a Mathematical and Physical Character, 1929, 125(797): 330-344.

Sezgin, J. G., Bosch, C., Montouchet, A., et al. Modelling of hydrogen induced pressurization of internal cavities. International Journal of Hydrogen Energy, 2017, 42(22): 15403-15414.

Shoghl, S. N., Naderifar, A., Farhadi, F., et al. Prediction of Joule-Thomson coefficient and inversion curve for natural gas and its components using CFD modeling. Journal of Natural Gas Science and Engineering, 2020, 83: 103570.

Smith, J. M., Van Ness, H. C., Abbott, M. M., et al. Introduction to Chemical Engineering Thermodynamics, 9th Edition. New York, USA, McGraw-Hill, 2022.

Song, B., Wang, X., Liu, Z. Gaseous transport properties of hydrogen, deuterium and their binary mixtures from ab initio potential. Molecular Physics, 2013, 111(1): 49-59.

Spycher, N. F., Reed, M. H. Fugacity coefficients of H_2, CO_2, CH_4, H_2O and of H_2O-CO_2-CH_4 mixtures: A virial equation treatment for moderate pressures and temperatures applicable to calculations of hydrothermal boiling. Geochimica et Cosmochimica Acta, 1988, 52(3): 739-749.

Stiel, L. I., Thodos, G. The thermal conductivity of nonpolar substances in the dense gaseous and liquid regions. AIChE Journal, 1964, 10(1): 26-30.

Striednig, M., Brandstätter, S., Sartory, M., et al. Thermodynamic real gas analysis of a tank filling process. International Journal of Hydrogen Energy, 2014, 39(16): 8495-8509.

Sun, E., Sun, Y., Feng, S., et al. Thermodynamic study of organic Rankine cycle based on extraction steam compression regeneration in the supercritical state. Energy Conversion and Management, 2023, 293: 117546.

Tkacz, M., Litwiniuk, A. Useful equations of state of hydrogen and deuterium. Journal of Alloys and Compounds, 2002, 330: 89-92.

Tosun, I. The Thermodynamics of Phase and Reaction Equilibria. Alpharetta, USA, Elsevier, 2021.

Townend, D. T. A., Bhatt, L. A. Isotherms of hydrogen, carbon monoxide and their mixtures. Royal Society, 1931, 134(824): 502-512.

Thermodynamics Research Center (TRC). Thermodynamic Tables-Hydrocarbons. The Texas A&M University Sys-

tem, College Station, TX, 1986.

Tsederberg, N.V., Popov, V.N., Andreev, I.I. Experimental investigation of the viscosity of hydrogen, Teploenergetika, 1965, 12(4): 84-85. (in Russian)

United Nations Industrial Development Organization (UNIDO). On the sidelines of the 24th Session of the Conference of the Parties to the United Nations Framework Convention on Climate Change (UNFCCC)-COP24. 2018, p. 12.

Verschoyle, T. T. H. Isotherms of hydrogen, of nitrogen, and of hydrogen-nitrogen mixtures, at 0° and 20 °C, up to a pressure of 200 atmospheres. Royal Society, 1926, 111(759): 552-576.

Wang, H., Xin, Y., Kou, Z., et al. Numerical study of the efficiency of underground hydrogen storage in deep saline aquifers, rock springs uplift, Wyoming. Journal of Cleaner Production, 2023, 421: 138484.

Wang, Y., Aryana, S. A. Coupled confined phase behavior and transport of methane in slit nanopores. Chemical Engineering Journal, 2021, 404: 126502.

Wei, C., Raad, S. M. J., Leonenko, Y., et al. Correlations for prediction of hydrogen gas viscosity and density for production, transportation, storage, and utilization applications. International Journal of Hydrogen Energy, 2023, 48(89): 34930-34944.

Wiebe, R., Gaddy, V. L. The compressibilities of hydrogen and of four mixtures of hydrogen and nitrogen at 0, 25, 50, 100, 200 and 300 and to 1000 atmospheres. Journal of the American Chemical Society, 1938, 60(10): 2300-2303.

Xue, Y., Zhang, L., Zhang, S., et al. Analysis of low emission characteristics of NH_3/H_2/air mixtures under low temperature combustion conditions. Fuel, 2023, 337: 126879.

Yang, Z., Liu, Z., Zhou, J., et al. A graph neural network (GNN) method for assigning gas calorific values to natural gas pipeline networks. Energy, 2023, 278: 127875.

Yusibani, E., Nagahama, Y., Kohno, M., et al. A capillary tube viscometer designed for measurements of hydrogen gas viscosity at high pressure and high temperature. International Journal of Thermophysics, 2011, 32: 1111-1124.

Zhang, T., Liu, J., Sun, S. Technology transition from traditional oil and gas reservoir simulation to the next generation energy development. Advances in Geo-Energy Research, 2023, 7(1): 69-70.

Zheng, J., Zhang, X., Xu, P., et al. Standardized equation for hydrogen gas compressibility factor for fuel consumption applications. International Journal of Hydrogen Energy, 2016, 41(15): 6610-6617.